Space based space surveillance using passive radio frequency observations – A feasibility study

Edwin G. W. Peters,
Timothy Bateman, Rabbia Saleem, Andrew Lambert, Melrose Brown
UNSW Canberra Space, Canberra, Australia

ABSTRACT

Space-based space surveillance (SBSS) is a growing area of interest, and an obvious way to extend the coverage of parts of the sky and Earth's orbits that are not visible from terrestrial sensors. While the majority of current space-based sensors focus on Earth or planetary observations, there are a limited number of optical SBSS sensors, such as NEOSSat, Saphire and GASSP, as well as sensors used for object inspection. Optical sensors in space are not affected by weather effects in Earth's atmosphere, greatly increasing their operational capabilities. However, the field of view of optical sensors is narrow, which limits the feasibility of using these sensors for surveillance. A number of optical SBSS sensors are utilised for object inspection, where specific objects are inspected. Space based passive RF sensors would provide the large coverage that terrestrial sensors provide, with the prospect of using these to detect unknown objects as well as monitor existing objects. Constellations of passive RF equipped spacecraft in orbit, and around the moon can sense a large part of the sky. Thus, SBSS has the prospect of providing crucial capability essential for object detection, high precision localisation, monitoring and manoeuvre detection in space.

These spacecraft can be equipped with a multitude of sensors, such as wide beamwidth detection sensors, as well as narrow beamwidth RF, optical and event based precision sensors. While space based sensors exist today, the majority are utilised for Earth observations. Challenges however arise; What orbits provide the best coverage? How should the apertures be sized and configured? Power and size requirements of the spacecraft. In this work, we present a feasibility study on the prospect of space based space surveillance (SBSS). The feasibility study is backed by RF signal collections performed using the software defined radios onboard the M2 spacecraft.

The University of New South Wales, Canberra (UNSW Canberra) embarked on an ambitious Cube Satellite research, development, and education program in 2017 through funding provided by the Royal Australian Air Force (RAAF). M2 is the final mission of the series, comprising of two identical spacecraft that were launched on the 22nd of March 2021 in a 45 degree inclination 550 km altitude orbit. This current work will use data from the passive RF collection campaign on our M2 spacecraft to inform a feasibility study for a dedicated LEO space-based passive RF sensor capability. The goals of this study is to investigate how a passive RF based SBSS capability can augment a ground network of sensors to provide global coverage of Earth's and cis-lunar orbits. We will investigate different RF sensor and orbit configurations and provide a feasibility study for a dedicated passive RF based SBSS spacecraft. We will investigate joint operations with combinations of wide field of view passive RF sensors and narrow field of view sensors, such as high gain RF antennas and optical sensors to provide new capabilities for monitoring, object and manoeuvre detection in both LEO and other orbits.

1. INTRODUCTION

The number of near-Earth resident space objects is set to grow by an order of magnitude by the end of the decade[4, 17, 18]. Developing new space traffic management (STM) systems is critical to mitigate the risk of on-orbit collisions from the rapidly growing population of spacecraft. Future STM systems

must contend with not only an increase in the number of objects in orbit but an increasingly dynamic space environment, where low-thrust electric propulsion systems combined with artificial intelligence-based spacecraft navigation systems result in levels of manoeuvrability that were not envisioned during the design of existing STM systems. The emergence of commercial space actors as the primary owner/operators of future satellite technology has driven the transition of STM from a military responsibility to the civilian realm. It is therefore critical that new space domain awareness (SDA) sensors and mission systems are developed from the civilian and commercial sector to meet both the technical and business/use case challenges that the changing utilisation of the space domain requires. With propulsion and passive manoeuvring becoming feasible for small spacecraft in the low Earth orbit (LEO) regime, the need for tracking and manoeuvre detection increases substantially. Accurate tracking and manoeuvre detection is even more essential, when potentially non-collaborative spacecraft operate in close proximity to each other [2].

There is an increasing development of terrestrial SDA sensors through Australian efforts, such as [22, 7] that use passive radio frequency (RF) and passive radar to track LEO objects. Multi-static radar tracking is also deployed on multiple continents to achieve a greater cover of the LEO regime [15]. While terrestrial SDA sensing has several advantages over space based sensing, such as supporting large apertures and computation facilities, it might be difficult to achieve global coverage using terrestrial sensors only. Geographical as well as geopolitical challenges limit locations where sensing sites can be deployed and thereby leave parts of the sky invisible. Additionally, observing and tracking cis-lunar and lunar targets from terrestrial sites can be challenging. Deploying sensing sites in space, onboard orbiting or stationary spacecraft enables coverage of parts of the sky that previously were difficult or impossible to access. Additionally, sensors can be deployed in higher orbits around Earth, around the moon or other planets in the solar system.

Space-based space surveillance (SBSS) missions with optical sensor capabilities have been demonstrated by the US Air Force through the SBSS mission, which operates in a sun-synchronous LEO [5], and are currently being demonstrated by various startup companies, such as HEO Robotics. RF sensing capabilities have, to the best of our knowledge, not been demonstrated for on-orbit SBSS operations. This work investigates the feasibility for small LEO satellites with simple sensors to perform passive RF sensing for SBSS capabilities.

Sensor tasking for SBSS spacecraft featuring a combination of wide field of view (FOV), such as omni directional RF antennas and narrow FOV sensors, such as high-gain antennas, phased arrays or optical sensors is considered in [24, 23]. These works consider two SBSS spacecraft tracking a target using time difference of arrival (TDoA) and frequency difference of arrival (FDoA) measurements. Gaussian mixture models are used to describe the feasible region where the target could reside an model measurement uncertainty of the wide FOV sensors. Strategies are then designed to search this probability space to task narrow FOV sensors to locate the target. Future work will combine sensor tasking with direct SBSS mission concepts and feasibility.

This paper is organised as follows: Section 2 discusses passive RF for SBSS. Section 3 presents two case studies for passive RF mission concepts and the observability of a number of LEO targets. Constellations of spacecraft are discussed in Section 4. Utilising emitters of opportunity to utilise passive radar is discussed in Section 5. The study is summarised in Section 6.

2. PASSIVE RF FOR SBSS

When detecting RF signals, the received signal to noise ratio (SNR) needs to be sufficiently high to trigger a detection. While techniques, such as coherent and non-coherent integration can be used to some extend to increase the received SNR, the power received at the SBSS spacecraft is limited by the power radiated from the target spacecraft including any directivity from the antenna apertures on the target spacecraft.

The design decisions for the antenna payloads on a SBSS mission will need to take directivity into account as well. While omnidirectional antennas allow one to collect signals from any direction, terrestrial interference is also collected, and increases the risk that power emitters mask low power emitters, effectively rendering the target invisible. Omnidirectional antennas also feature low antenna gains. Narrow beamwidth antennas feature higher gain, allowing the detection of weaker signals. These also reject interference outside of the antenna beam, which can make the system robust to terrestrial interference and jamming. While directional antennas need to be pointed in the direction where signals of interest are to be captured, the pointing information can be used to constrain the feasibility region where the target that emits RF signals can

antenna configuration	visibility	gain	interference rejection	what can be measured
omnidirectional	360°	low	poor	Signal charactersistics, FoA
single high gain	narrow	higher	improved	Signal charactersistics, FoA, coarse AOA
multiple high gain	potentially omnidirectional	higher	good	Signal charactersistics, FoA, improved AOA
phased array	narrow with very narrow focus	very high	very good	Signal charactersistics, FoA, fine AOA, signal separation

Table 1: Coarse overview of antenna configurations and the information that can be extracted

reside. Multiple narrow beam width antennas can be placed around the SBSS spacecraft body to enable omnidirectional cover while allowing passive interference rejection through antenna directivity, or active interference rejection through signal processing techniques. Additionally, multiple antennas can be used to determine the angle of arrival (AOA) of an RF signal, further reducing the feasibility region.

Passive RF sensing can obtain multiple measurements. Table 1 provides a coarse overview over the information that can be extracted from the RF signals when various antenna configurations are used for sensing. The frequency of arrival (FoA) and signal characteristics, such as power, bandwidth, modulation scheme, characteristics and potential fingerprints can be extracted from any captured RF signal. Generally, increased receive SNR, which can be obtained by increasing the antenna gain improves the quality of these parameters. As Table 1 indicates, utilising multiple antennae allows additional measurements while improving gain and interference rejection.

Position determination of a target based of measurements is typically done using orbit determination software. With the position of the SBSS spacecraft known, for example using global navigation satellite system (GNSS) receivers and star trackers, the orbit of target spacecraft can be determined using tools, such as GMAT [11], Orekit [13, 14] or STRF [1]. Multiple algorithms can be used for signal detection, Doppler estimation and signal identification. This includes spectral signal processing methods, such as presented in [20, 25, 21], spectral averaging methods [10] or direct tracking methods, such as Costa's loops or phase locked loops (PLLs) [12, 6]. Machine learning methods can also be utilised for signal detection and identification [16]. While being a crucial aspect in mission design, the computational requirements, necessary hardware and power and heat constraints are omitted in the current case study.

2.1 Link budget

For a signal emitted by a target spacecraft to be detectable by a SBSS spacecraft, the received SNR needs to be sufficient, such that the target's RF emission can be separated from the noise. The received SNR depends directly on the RF power intensity emitted towards the SBSS spacecraft. This can be very low when the target spacecraft utilises high gain, narrow beamwidth antennas that are pointed towards other spacecraft or ground stations. In these situations the SBSS spacecraft potentially has to resort to capture side-lobe emissions, which are significantly lower, often 10s of dB, than the main lobe.

In this section, we establish the maximum range of detectability for a number of LEO spacecraft based on their known or guessed RF emission parameters. The range of detectability is determined by the received SNR on the SBSS spacecraft being above a set threshold.

The power received for an RF link is given by

$$P_r = P_t - L + G - \mathrm{FSPL}, \tag{1}$$

where P_r is the power received, P_t the power transmitted in dBW, L and G are the losses and gains in the RF systems, respectively, and FSPL the free space path loss (FSPL), given by

$$\mathrm{FSPL} = 10\log_{10}\left(\frac{4\pi r}{\lambda}\right), \tag{2}$$

polarisation loss	frontend loss	noise temperature	CPI
L_{pol}	L_{rx}	t	G_{CPI}
3 dB	1 dB	300 K	0 dB

Table 2: Receiver parameters used for the RF link budget.

Frequency band	Aperture gain	band	Comments
VHF	1.5 dBi	30 MHz to 300 MHz	wide-band omnidirectional, linear polarisation
UHF	2 dBi	300 MHz to 1000 MHz	wide-band omnidirectional, linear polarisation
S-band	6 dBi	2 GHz to 4 GHz	60° patch circular polarisation
X-band	6 dBi	8 GHz to 12 GHz	60° patch circular polarisation

Table 3: The antenna configurations considered for the SBSS spacecraft.

with $\lambda = c/f$ the wavelength where $c = 2.99 * 10^8$ m/s and f the RF carrier frequency in Hz. The range or distance in meter is denoted by r. Note that capital case letters indicate units in dB while low case letters indicate linear units. The SNR of a received signal is given by

$$\text{SNR} = P_r - P_n, \tag{3}$$

where $P_n = 10\log_{10}(p_n)$ is the thermal noise with $p_n = ktB$, with $k = 1.380649 * 10^{-23}$ J/K is the Boltzmann constant, t the temperature in K, and B the noise bandwidth in Hz.

The maximum range at which a spacecraft can be detected at with a certain SNR, $\overline{\text{SNR}}$, can then be found by combining (1) and (3) and solving for the FSPL, which yields

$$\text{FSPL} = P_t - L + G - P_n - \overline{\text{SNR}}. \tag{4}$$

Then, the maximum distance $d_{\max}$ where the SNR is higher than $\overline{\text{SNR}}$ for any range $r \leq r_{\max}$ is found by isolating r in (2). This yields

$$r_{\max} = \sqrt{\text{fspl}}\frac{\lambda}{4\pi}, \tag{5}$$

with $\text{fspl} = 10\log_{10}(\text{FSPL})$ being the FSPL in linear units. Combining (4) and (5) results in

$$r_{\max} = \sqrt{10^{\frac{P_t - L + G - P_n - \overline{\text{SNR}}}{10}}}\frac{\lambda}{4\pi}. \tag{6}$$

The losses L typically consist of the polarisation mismatch L_{pol} and internal losses on the receiver L_{rx}. The gains G include the receive antenna gain G_{rx} and processing gain due to coherent integration time G_{CPI} as well as other processing gains.

Table 4 shows the maximum detection range for a number of LEO spacecraft when a minimum detection SNR of 15 dB is desired using the RF parameters shown in Table 2 and antenna configuration shown in Table 3. If coherent integration is used to accumulate energy, the maximum range can increase by up to

$$r_{\max}(G_{\text{CPI}}) = r_{\max}\sqrt{10^{\frac{G_{\text{CPI}}}{10}}}. \tag{7}$$

Likewise, changing the SNR threshold affects the maximum range by a factor $\sqrt{10^{\frac{\text{change in SNR}}{10}}}$.

3. CASE STUDIES FOR A CONCEPT MISSION FOR SBSS USING PASSIVE RF

In this section, we consider two concept mission designs for SBSS. The first concept is based on a lower inclination LEO mission, while the other is based on a sun-synchronous LEO mission. For both missions,

spacecraft name	period	inclination	apogee	perigee	carrier	bandwidth	EIRP	max range
NOAA 15	100.95 min	98.6 °	812 km	796 km	137 MHz	35 kHz	7.0 dBW	3430 km
NOAA 18	101.91 min	98.91 °	860 km	839 km	137 MHz	35 kHz	7.0 dBW	3430 km
NOAA 19	101.92 min	99.09 °	860 km	839 km	137 MHz	35 kHz	7.0 dBW	3430 km
METEOR-M2 3	101.13 min	98.76 °	814 km	810 km	137.9 MHz	72 kHz	3.0 dBW	1682 km
ZHUHAI-1 02	94.82 min	43.02 °	518 km	502 km	145.9 MHz	4.8 kHz	0.0 dBW	5487 km
ISS	92.9 min	51.64 °	420 km	413 km	437.8 MHz	10 kHz	3.0 dBW	1421 km
CREW DRAGON 7	97.9 min	51.64 °	420 km	413 km	444.925 MHz	10 kHz	3.0 dBW	1399 km
CAPELLA-11	97.62 min	53.01 °	649 km	641 km	9.6 GHz	300 MHz	18.3 dBW	666 km
PROGRESS-MS 24	92.9 min	51.64 °	420 km	413 km	146 MHz	12 kHz	0.0 dBW	3468 km
OBJECT D	98.8 min	45 °	704 km	691 km	437 MHz	4 kHz	0.0 dBW	2007 km
OBJECT B	98.8 min	45 °	706 km	697 km	437 MHz	30 kHz	3.0 dBW	822 km
CYGNUS NG-19	92.9 min	51.64 °	420 km	413 km	437 MHz	15 kHz	3.0 dBW	1163 km
M2 PATHFINDER	96.35 min	97.76 °	593 km	575 km	450 MHz	15 kHz	0.0 dBW	1006 km
M2-A	95.09 min	45 °	532 km	512 km	450 MHz	15 kHz	0.0 dBW	1006 km

Table 4: Satellites maximum range for detection with at least 15 dB SNR with the capturing parameters listed in Tables 2 and 3.

spacecraft name	low inclination orbit			SSO		
	avg. obs interval	max obs interval	avg pass	avg. obs interval	max obs interval	avg pass
NOAA 15	2.9 hr	22.0 hr	277 s	1.9 hr	21.4 hr	252 s
NOAA 18	4.4 hr	20.5 hr	344 s	4.2 hr	24.8 hr	331 s
NOAA 19	3.4 hr	19.7 hr	293 s	2.8 hr	22.3 hr	278 s
METEOR-M2 3	3.4 hr	21.2 hr	298 s	3.2 hr	26.3 hr	289 s
ZHUHAI-1 02	no passes in range			5.1 hr	78.9 hr	553 s
ISS	4.2 hr	57.9 hr	440 s	3.3 hr	34.7 hr	287 s
CREW DRAGON 7	4.1 hr	57.1 hr	429 s	3.3 hr	34.7 hr	284 s
CAPELLA-11	4.1 hr	49.7 hr	339 s	1.4 hr	57.4 hr	254 s
PROGRESS-MS 24	4.1 hr	57.1 hr	429 s	3.3 hr	34.7 hr	284 s
OBJECT D	4.2 hr	36.3 hr	379 s	2.1 hr	45.5 hr	260 s
OBJECT B	4.4 hr	35.5 hr	386 s	2.1 hr	44.7 hr	256 s
CYGNUS NG-19	4.1 hr	57.1 hr	429 s	3.3 hr	34.7 hr	284 s
M2-A	same orbital plane			5.0 hr	95.0 hr	569 s
M2 Pathfinder	5.0 hr	95.0 hr	569 s	same orbital plane		

Table 5: Pass info for low inclination orbit and SSO SBSS spacecraft over 10 days.

the spacecraft is considered to be of a smallsat size, and will feature small antenna apertures as listed in Table 3. The antenna gain for especially the lower frequency bands is low to allow for wide beamwidths. It is also worth noting that, as shown in Table 3, the Sband and Xband antennas have a 60° beamwidth. Thus, the SBSS spacecraft either has to point the antenna towards the targets, or multiple antennas have to be installed such that 360° cover is achieved. In this analysis, we consider that the SBSS spacecraft is oriented such that it has line-of-sight (LOS) visibility of all targets at any time. As discussed in Section 2, a coarse AOA can be estimated when multiple antennas are used.

3.1 Low inclination orbit concept

The orbit inclination for the low inclination SBSS mission is based of the M2 orbit, which is described in Table 6.

Observation parameters to the LEO spacecraft shown in Table 4 are shown in Table 5. The average observation interval across all satellites listed is 4.025 hr, with an average pass time of 367 s. While ZHUHAI-1 02 is not visible at all within the 10 days simulated, the worst case time between 2 observations is 95 hr for M2 Pathfinder, which has the same orbit as the SSO SBSS mission. The next longest observation interval is 57.1 hr for PROGRESS-MS 24. The average worst case interval between two observations is 44 hr while the median is 43 hr.

The LOS distance over those 10 days for the NOAA and METEOR-M2 3 spacecraft and the SBSS spacecraft

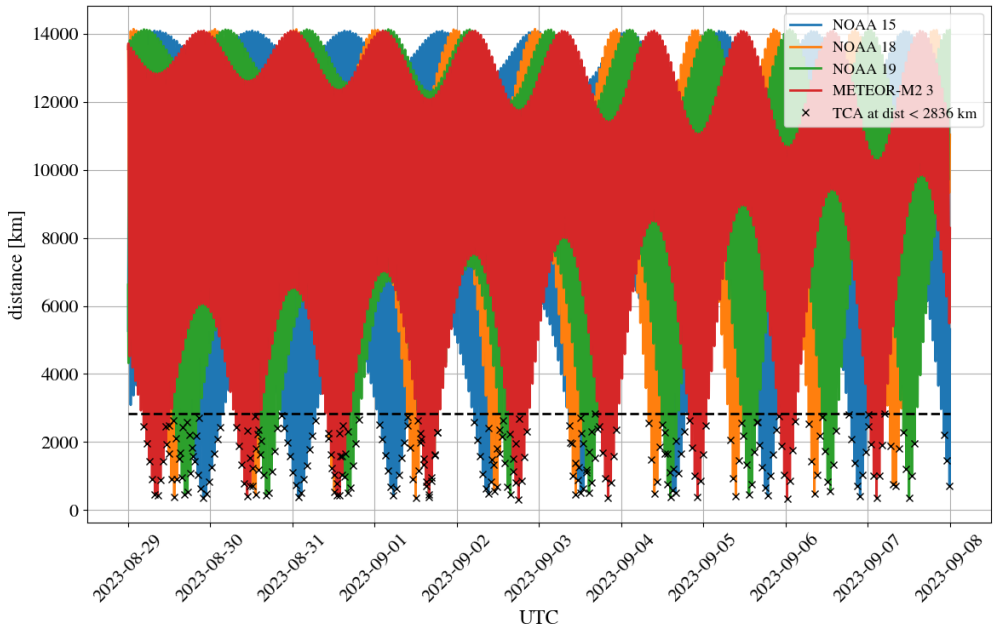

Fig. 1: LOS to weather satellites from SBSS spacecraft with orbit described in the left column in Table 6

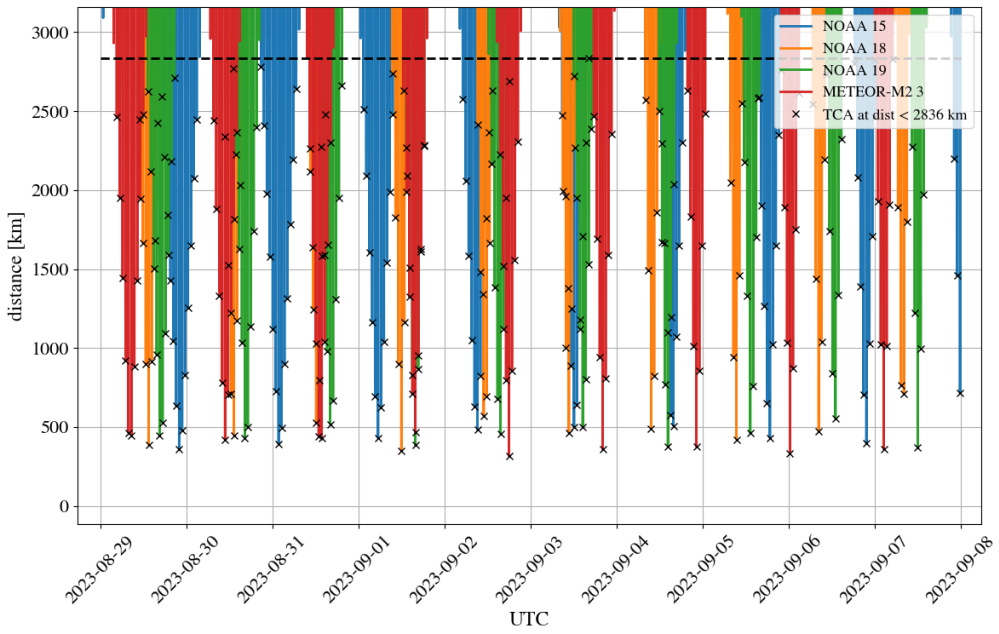

Fig. 2: LOS to weather satellites from SBSS spacecraft with orbit described in the left column Table 6

	low inclination spacecraft M2-A	SSO spacecraft M2 Pathfinder
Inclination	45°	97.76°
Apogee	532 km	593 km
Perigee	512 km	575 km
Period	95.09 minute	96.35 minute

Table 6: Orbital parameters for SBSS missions

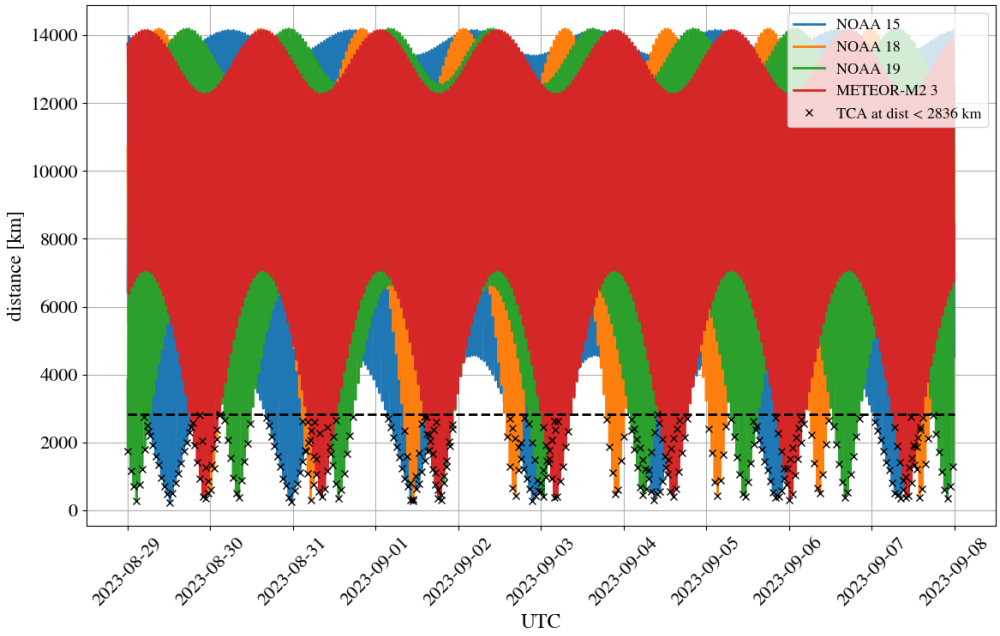

Fig. 3: LOS to weather satellites from SSO SBSS spacecraft with orbit described in the right hand column in Table 6

is shown in Figs. 1 and 2. The dashed line is the range threshold for a SNR of 15 dB based on the parameters of the spacecraft listed in Table 4 and antenna configuration in Table 3. Figure 2 zooms in on the sections where the LOS range is within the maximum range $r_{\max}$ where the SNR is higher than the lower threshold $\overline{\text{SNR}}$ of 15 dB.

3.2 Sun synchronous orbit concept

The second SBSS mission concept is based on a spacecraft in a low SSO. The parameters of the M2 Pathfinder spacecraft are used, which are shown in Table 6. The antenna configuration and other assumptions are identical to the low inclination mission concept, described in Section 3.1.

The average and worst case observation intervals over 10 days as well as the average pass length are shown in Table 5. For an SBSS spacecraft in a SSO, the average observation interval is 3.15 hr, which is almost 25 % shorter than the low inclination orbit SBSS spacecraft. The worst case time between two observations is 95 hr for M2-A, which has the same orbit as the low inclination SBSS spacecraft. The average worst case observation interval is 42.7 hr, while the median is 34.7 hr. Also, it is noteworthy that the SSO spacecraft can observe the ZHUHAI-1 02 target. The average pass length is 321 s, which is 10 % less than the low inclination spacecraft.

3.3 Summary

Table 7 compares the average numbers from the analysis presented in Table 6. The SSO SBSS mission presented in Section 3.2 features a higher revisit rate and significantly lower worst case intervals between observations. However, the average observation duration is 12 % shorter than the low inclination orbit SBSS

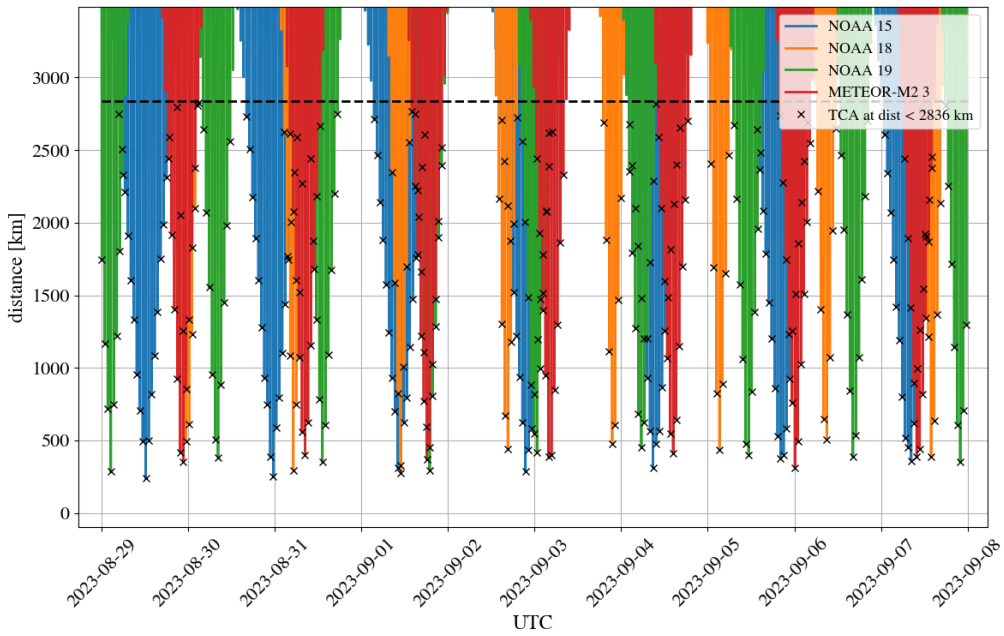

Fig. 4: LOS to weather satellites from SSO SBSS spacecraft with orbit described in the right hand column in Table 6

	avg. obs interval	mean max obs interval	median max obs interval	avg pass
Section 3.1	4.025 hr	44.09 hr	43.0 hr	367 s
Section 3.2	3.15 hr	42.7 hr	34.7 hr	321 s

Table 7: Average observation numbers for both SBSS missions

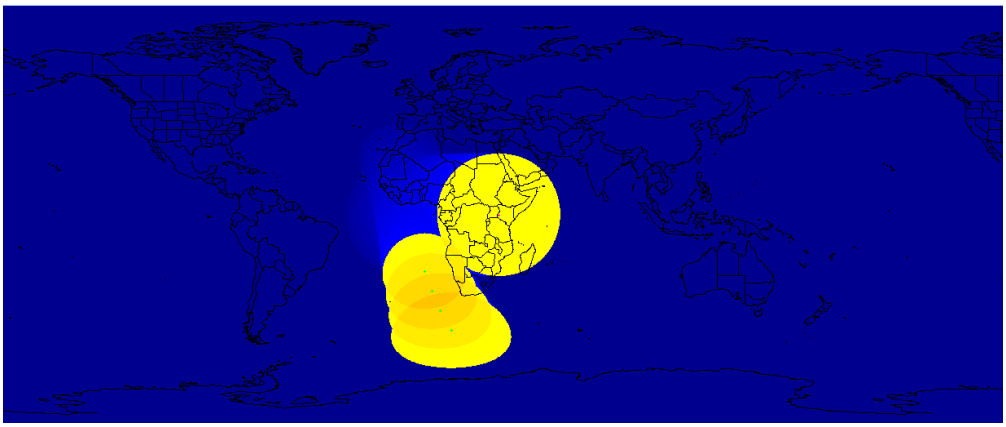

Fig. 5: Example coverage of a SBSS constellation with four spacecraft in one orbital plane and one target.

mission presented in Section 3.1. The low inclination orbit mission did not have any visible passes in range with the ZHUHAI-1 02 mission in the 10 days analysed. This is due to the spacecraft being in a very similar orbit altitude and inclination as the SBSS mission. Thus, the orbital phase change between the two spacecraft will progress slowly, resulting in extended periods of continuous LOS within range with long periods without a direct LOS between those.

From the two case studies, the SBSS spacecraft in an SSO provides higher visibility and revisit rates of potential target spacecraft compared to a low inclination SBSS mission. Generally, target spacecraft that have similar a similar orbital period and are out of phase will be difficult to track. This issue can be mitigated by using multiple spacecraft either in the same orbital plane or multiple orbital planes.

4. SBSS CONSTELLATIONS

Passive RF observations from direct emissions of target spacecraft were considered in Sections 2 and 3. Multiple spacecraft can be flown in a close formation, with LOS distances ranging from mere kilometres to 100s of kilometres. This allows parameters, such as the TDoA and FDoA to be measured [3, 19], allowing the target localisation using a significantly reduced number of measurements compared to pure Doppler or AOA [9].

An example constellation of four spacecraft in one orbital plane with 97.76° inclination and an apogee and perigee of 550 km and a single low inclination target is shown in Fig. 5. The time of periapsis between the SBSS spacecraft in the constellation is 143 s, equating to a LOS distance of 1072 km. The radius of the cover circles on the map for the constellation spacecraft corresponds to a range of 3500 km.

Accurate knowledge of the distance between the spacecraft in the SBSS constellation and their individual oscillator clock drift is crucial for accurate measurements. Typical oven controlled crystal oscillators (OCXOs) can feature frequency errors down to 0.003 ppm, but require substantial power to maintain the temperature constant. The range rate uncertainty due to the clock stability for OCXOs, thermally compensated crystal oscillators (TCXOs) and conventional crystal oscillators is shown in Table 8. In addition to FoA measurements on the single spacecraft, TDoA and FDoA measurements will also be affected by the oscillator stability.

While clock stability is crucial for accurate parameter estimation of target spacecraft, less stable oscillators can be utilised if their performance can be tracked. This can, for example, be done using global positioning system (GPS) disciplining or through the use of reference signals. Oscillator drift between the SBSS spacecraft can be characterised through, for example, ranging measurements.

	crystal oscillator	TCXO	OCXO
stability	±10 ppm	±0.5 ppm	±0.003 ppm
range rate error	3 km/s	149 m/s	0.9 m/s

Table 8: Range rate uncertainty for various crystal oscillator types.

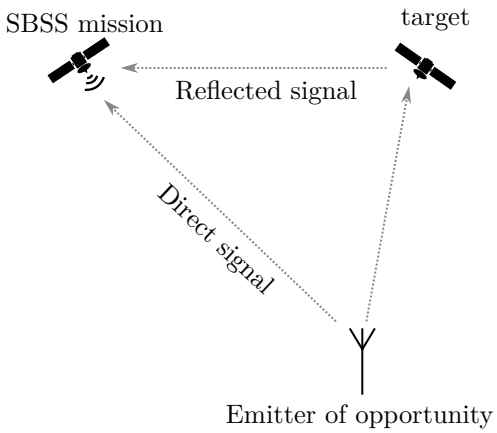

Fig. 6: Space based passive radar configuration using terrestrial emitter of opportunity.

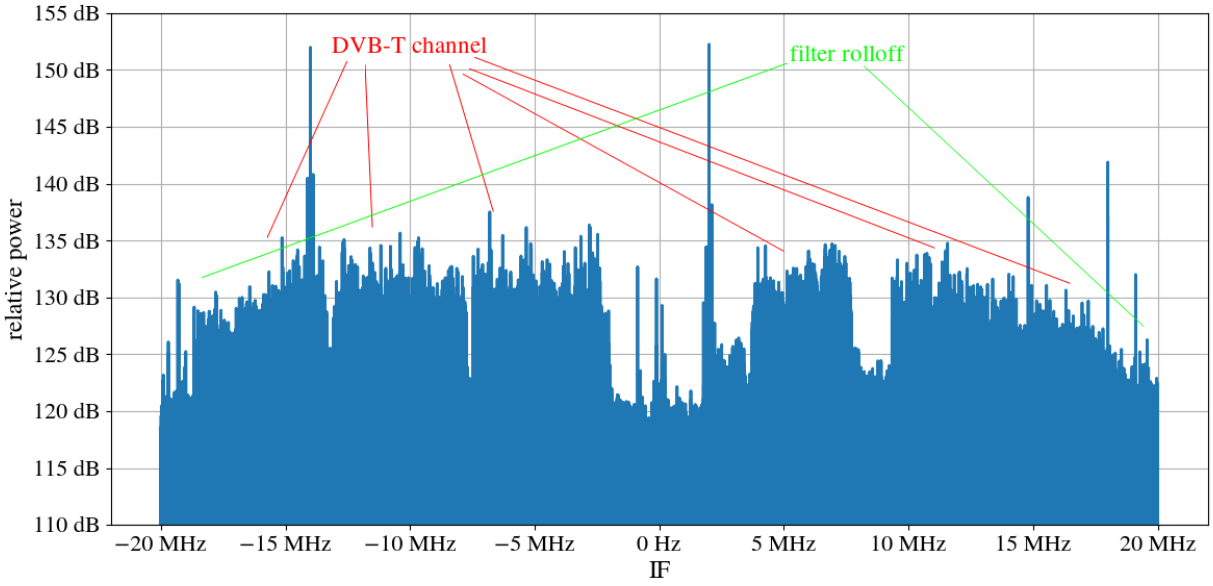

Fig. 7: DVB-T capture taken on M2-A at 197.5 MHz.

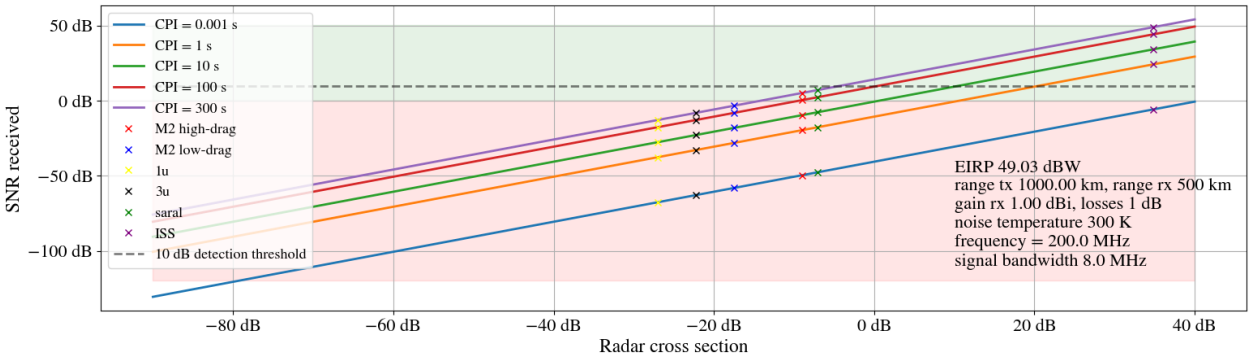

Fig. 8: Link budget for DVB-T passive radar with ideal illuminator with 80 kW EIRP.

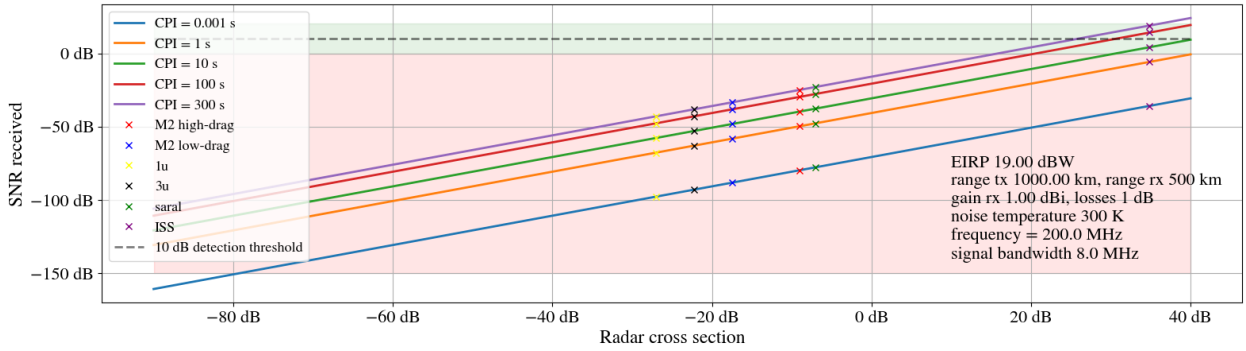

Fig. 9: Link budget for DVB-T passive radar with ideal illuminator with 73 W EIRP, based of SNR received by M2-A recording.

5. PASSIVE RADAR

While direct passive RF observations rely on the target to emit RF signals, an alternative is to use radar. Mono- and multi-static radar are typically used for terrestrial detection and tracking of objects in LEO. However, the radar signal requires a significant effective isotropic radiated power (EIRP) for target illumination. This can be achieved by using large RF power amplifiers or using narrow beamwidth antennas that achieve a high directive gain. Detecting small objects is also difficult due to the small radar signatures. Alternatively, terrestrial emitters of opportunity can be utilised as illuminators, enabling passive radar observations [8, 7]. Passive radar works in the way that a direct emission from the illuminator is captured as well as delayed and substantially weaker emissions that are reflected of targets. By cross correlating these emissions over sufficient time, a correlation peak indicates a detection. Knowledge of the Doppler rate, or a brute force search for the Doppler rate is required to achieve effective cross correlation output. A space based passive radar configuration using a terrestrial emitter of opportunity is illustrated in Fig. 6.

Well suited signals for passive radar exist in the FM and digital video broadcast – terrestrial (DVB-T) bands, which are used for broadcast radio and terrestrial digital TV, respectively. Both emissions reside in the very-high frequency (VHF) band, which yields high effective antenna areas. Additionally, DVB-T features wide beamwidth emissions. The signals can be reflected of targets and be captured by spacecraft in LEO. An example of the power spectral density (PSD) of a capture containing 6 DVB-T channels that was captured with the software defined radio (SDR) onboard the UNSW M2-A spacecraft is shown in Fig. 5. The SNR received exceeds 15 dB for each DVB-T channel. These DVB-T channels each have a bandwidth of 8 MHz. This would add a processing gain of 39 dB for 1 ms coherent processing interval (CPI) or 69 dB of processing gain for 1 s CPI.

Figure 8 shows a link budget for passive radar with an ideal EIRP of 80 kW emitted by the Canberra-based

Current SNR for Saral	−40 dB
Helix antenna	10 dB
4 spacecraft observing	6 dB
4 antennas per spacecraft	6 dB
10 DVB-T channels	10 dB
5 DVB-T emitters of opportunity	7 dB
Observe over 10 passes	10 dB
Total	9 dB SNR

Table 9: Passive radar example of improvements to measured signal strength to increase the detected SNR.

DVB-T broadcast emitter. The different lines show the received SNR for different CPIs. The range from the SBSS spacecraft and target to the emitter is considered to be 1000 km while the LOS distance between the SBSS spacecraft and target is 500 km. Only one emitting source and channel are considered. It is worth noting that the International Space Station (ISS), Saral ($1\,m^2$ area) and M2 in high drag, where the latter has an area of $0.09\,m^2$, are detectable. This however assumes that the radiation from the emitter is isotropic, which is not necessarily the case. Utilising all 6 channels that are depicted in the PSD in Fig. 7 can increase the processing gain by 7.8 dB. Including channels out of band of the spectrum in Fig. 7 and digital radio channels, it is estimated that a diversity gain of 10 dB can be achieved. Utilising all emitters of opportunity that are in LOS simultaneously can further increase the processing gain. The link budget shown in Fig. 8 is based of the assumption that a basic wide beamwidth antenna with 1 dBi gain is used on the SBSS spacecraft.

Using the range and parameters used for the link budget shown in Fig. 8, the SNR received at the M2 spacecraft on 1000 km range should be 45 dB for a 80 kW EIRP at the broadcast transmitter. This is 30 dB higher than the SNR detected, which was 15 dB. Based of the SNR received on the M2 SDR, the EIRP of the terrestrial broadcast emitter in the elevation of the M2 spacecraft was merely 18 dBW, or 73 W. Figure 9 shows a revised link budget analysis when an EIRP of 18 dBW is considered from the broadcast emitter. In this case, only the ISS is detectable when at 500 km range. Increasing the aperture on the SBSS spacecraft will increase the detectability of smaller objects. However, with a 300 s CPI, the SNR for a mid-sized spacecraft such as Saral is at −30 dB. For a 10 dB detection threshold, an additional 40 dB of gain is required. Some of this could be achieved by increasing the CPI. However, as illustrated in Figs. 2 and 4, the observation time for when the range is less than 500 km tends to be short. The observations can be performed across multiple pass windows. Additionally, a larger aperture can be used on the SBSS spacecraft. However, the physical size of the spacecraft limits the maximum size of the antennas. For example, a parabolic antenna with a diameter of 70 m would be required to achieve 41 dB of gain at 200 MHz. Table 9 shows an example of a configuration that can achieve 39 dB of gain. Even with sufficient a-priory knowledge, the computational requirements would be excessive and challenging to perform on-orbit with current technology and power requirements.

The processing of passive radar signals is typically done using cross correlations of the direct signal with the reflected signal. For the cross correlations to be effective, a-priory knowledge of frequency offsets, such as Doppler, oscillator drift and Doppler rate are required. A search grid can be utilised to find these parameters as part of an integer optimisation problem. This is however computationally intensive and requires significant computational resources to be addressed in real-time.

Further data collection and spectrum surveying from orbit are required to form a more comprehensive analysis of the requirements for the RF design on the SBSS spacecraft. Especially the power signatures of emitters of opportunity in the DVB-T spectrum needs to be mapped. The emissions that reach orbit are highly dependent on the transmitter antenna design, which tend to aim at focusing the energy horizontally rather than vertically. The mapping of DVB-T emissions also provides a coverage map, showing where passive radar using DVB-T signals can be feasible. Additionally, the computational requirements for processing passive radar data over longer CPI tend to be large, requiring high performance computational hardware and substantial power delivery and storage systems onboard a SBSS spacecraft with passive radar capabilities. It is also worth investigating ultra-high frequency (UHF) and Global System for Mobile communication

(GSM) band emitters of opportunity. Higher frequencies allow apertures with smaller physical size while maintaining the directivity due to the decrease of the wavelength of the RF signal. Additionally, antennas can be positioned physically closer to each other, allowing more antennas to be placed on a single spacecraft.

6. SUMMARY

We presented case studies for space-based space surveillance (SBSS) missions for low Earth orbit (LEO) that rely on passive radio frequency (RF) sensing. Here, we investigated detection ranges for various target types emitting RF signals at various bands and intensities. Orbit simulations were performed to map observation windows for a sun-synchronous orbit (SSO) and a low inclination orbit. The observation windows, where the target spacecraft are within detection range of the SBSS spacecraft were analysed. This includes the average length of observation windows, the frequency of these and the longest time between observations over a 10 day period. While both orbits showed frequent observations and observation window lengths averaging over 5 minutes, the SSO orbit case study generally showed higher revisit rates and shorter worst case times between observations.

Small constellations of SSO spacecraft were considered for multi-aperture analysis, such as time difference of arrival (TDoA) and frequency difference of arrival (FDoA). Clock source requirements were also considered in this study.

An analysis of utilising emitters of opportunity as illuminators for space-based passive radar was performed. Feasibility was analysed based on a spectrum survey performed using data captured on-orbit using the UNSW built and operated M2 spacecraft. While large targets, such as the International Space Station can be detected using simple antenna apertures, further studies are required to detect smaller targets and micro satellites.

Future work includes further spectral analysis of on-orbit signal captures from emitters of opportunity and potential target spacecraft for passive RF observations.

[1] Cees Bassa. STRF: satellite tracking toolkit for radio observations (RF) toolbox, 2020. `https://github.com/cbassa/strf`.

[2] Melrose Brown, Russell Boyce, Andrew Lambert, Edwin G. W. Peters, Steve Gehly, Samuel Boland, Ryan Jeffreson, Anthony Kremor, Timothy Bateman, Chris Capon, Brenton Smith, George Bowden, Lauren Glina, Lily Qiao, Sudantha Balage, Komal Gupta, Rizka Purwanto, Travis Bessell, Tom Reddell, James Bennett, Michael Lachut, and Tim McLaughlin. Formation flying and change detection for the UNSW canberra space 'm2' low earth orbit formation flying cubesat mission. In Advanced Maui Optical and Space Surveillance Technologies Conference, 2022.

[3] Liu Congfeng and Yun Jinwei. A joint TDOA/FDOA localization algorithm using bi-iterative method with optimal step length. Chinese Journal of Electronics, 30(1):119–126, 2021.

[4] Giacomo Curzi, Dario Modenini, and Paolo Tortora. Large constellations of small satellites: A survey of near future challenges and missions. Aerospace, 7(133), 2020.

[5] eoPortal. Sbss (space-based surveillance system), August 2022. `https://www.eoportal.org/satellite-missions/sbss#mission-status`.

[6] Farzan Farhangian and RenÃ© Landry. Multi-constellation software-defined receiver for doppler positioning with LEO satellites. Sensors, 20(5866), 2020.

[7] Daniel Finch, James Palmer, James Cooper, Daniel Oltrogge, and Thomas Johnson. Assessing passive radar for LEO SSA. In Advanced Maui Optical and Space Surveillance Technologies Conference, 2022.

[8] Brendan Hennessy, Mark Rutten, Robert Young, Steven Tingay, Ashley Summers, Daniel Gustainis, Brian Crosse, and Marcin Sokolowski. Establishing the capabilities of the murchison widefield array as a passive radar for the surveillance of space. Remote Sensing, 14(2571), 2022.

[9] Hatem Hmam. Optimal sensor velocity configuration for TDOA-FDOA geolocation. IEEE Transactions on Signal Processing, 65:628–637, 2017.

[10] Mohd Noor Islam, Thomas Q. Wang, Samuel Wade, Travis Bessell, Tim Spitzer, and Jeremy Hallett. Doppler and angle of arrival estimation from digitally modulated satellite signals in passive RF space domain awareness. In Advanced Maui Optical and Space Surveillance Technologies Conference, 2021.

[11] Moriba Jah, Steven Hughes, Matthew Wilkins, and Tom Kelecy. The general mission analysis tool (GMAT): A new resource for supporting debris orbit determination, tracking and analysis. In Proceedings of the Fifth European Conference on Space Debris, 2009.
[12] Joe J. Khalife and Zaher M. Kassas. Receiver design for doppler positioning with leo satellites. In ICASSP 2019 - 2019 IEEE International Conference on Acoustics, Speech and Signal Processing (ICASSP), pages 5506–5510, May 2019.
[13] Luc Maisonobe, Pascal Parraud, Maxime Journot, and Albert Alcarraz-Garcia. Multi-satellites precise orbit determination, an adaptable open-source implementation. In 2018 SpaceOps Conference, 2018.
[14] Luc Maisonobe, Véronique Pommier, and Pascal Parraud. Orekit: An open source library for operational flight dynamics applications. In 4th International Conference on Astrodynamics Tools and Techniques, pages 3–6, 2010.
[15] Darren McKnight, Erin Dale, Rachit Bhatia, and Mohin Patel. A map of the statistical collision risk in LEO. In Advanced Maui Optical and Space Surveillance Technologies Conference, 2022.
[16] Olusiji O Medaiyese, Abbas Syed, and Adrian P Lauf. Machine learning framework for RF-based drone detection and identification system. In 2021 2nd International Conference On Smart Cities, Automation & Intelligent Computing Systems (ICON-SONICS), pages 58–64, Oct 2021.
[17] NASA. Orbital debris, May 2021. `nasa.gov/mission_pages/station/news/orbital_debris.html`.
[18] Union of Concerned Scientists. Satellite database, May 2022. `https://www.ucsusa.org/resources/satellite-database`.
[19] Brian O'Keefe. Finding location with time of arrival and time difference of arrival techniques. ECE Senior Capstone Project, 2017.
[20] Edwin G. W. Peters, Timothy Bateman, Rabbia Saleem, Melrose Brown, and Andrew Lambert. A software defined radio based method for accurate frequency estimation for space domain awareness in real-time. In Advanced Maui Optical and Space Surveillance Technologies Conference, 2022.
[21] Edwin G. W. Peters and Craig R. Benson. A Doppler correcting software defined radio receiver design for satellite communications. IEEE Aerospace and Electronic Systems Magazine, 35(2):38–48, Feb 2020.
[22] Edwin G. W. Peters, Melrose Brown, Andrew Lambert, Lauren Glina, Timothy Bateman, Ed Kruzins, Rabbia Saleem, Travis Bessell, Tim Spitzer, Tom Wang, Kriti Tripathi, Damian Huxtable, Michael Soire, Simon Zinsli, Thomas Powles, Isabella Federle, Mark Aragon, Adam Haskard, Mark Thompson, Warren Nielsen, and Russell Boyce. A sensor network for integrated space traffic management for australia. In Advanced Maui Optical and Space Surveillance Technologies Conference, 2022.
[23] Andrew J. Sinclair, Edwin G. W Peters, and Melrose Brown. Narrow field-of-view sensor tasking for search of Gaussian-mixture probability density functions. In Astrodynamics Specialist Conference, 2023.
[24] Andrew J. Sinclair, Edwin G. W Peters, Joseph T. A. Peterson, and Melrose Brown. Probabilistic initial orbit determination from radio frequency measurements using Gaussian mixture. In Advanced Maui Optical and Space Surveillance Technologies Conference, 2023.
[25] Zhaowei Zhang, Hui Liu, Jun Yin, and Xiaoye Shi. Clustering-FFT based doppler-shift acquisition for space communications. IEEE Transactions on Communications, 70(2):1168–1182, Feb 2022.